JOURNAL OF THE ROYAL SOCIETY Interface

Development of colour-producing β-keratin nanostructures in avian feather barbs

Richard O Prum, Eric R Dufresne, Tim Quinn and Karla Waters

J. R. Soc. Interface 2009 **6**, S253-S265
doi: 10.1098/rsif.2008.0466.focus

Interface focus

J. R. Soc. Interface (2009) **6**, S253–S265
doi:10.1098/rsif.2008.0466.focus
Published online 23 February 2009

Development of colour-producing β-keratin nanostructures in avian feather barbs

Richard O. Prum[1,2,*], Eric R. Dufresne[3,4,5], Tim Quinn[6,†] and Karla Waters[6]

[1]*Department of Ecology and Evolutionary Biology,* [2]*Peabody Natural History Museum,*
[3]*Department of Mechanical Engineering,* [4]*Department of Chemical Engineering, and*
[5]*Department of Physics, Yale University, New Haven, CT 06511, USA*
[6]*Department of Ecology and Evolutionary Biology, University of Kansas, Lawrence, KS 66045, USA*

The non-iridescent structural colours of avian feather barbs are produced by coherent light scattering from amorphous (i.e. quasi-ordered) nanostructures of β-keratin and air in the medullary cells of feather barb rami. Known barb nanostructures belong to two distinct morphological classes. 'Channel' nanostructures consist of β-keratin bars and air channels of elongate, tortuous and twisting forms. 'Spherical' nanostructures consist of highly spherical air cavities that are surrounded by thin β-keratin bars and sometimes interconnected by tiny passages. Using transmission electron microscopy, we observe that the colour-producing channel-type nanostructures of medullary β-keratin in feathers of the blue-and-yellow macaw (*Ara ararauna*, Psittacidae) develop by intracellular self-assembly; the process proceeds in the absence of any biological prepattern created by the cell membrane, endoplasmic reticulum or cellular intermediate filaments. We examine the hypothesis that the shape and size of these self-assembled, intracellular nanostructures are determined by phase separation of β-keratin protein from the cytoplasm of the cell. The shapes of a broad sample of colour-producing channel-type nanostructures from nine avian species are very similar to those self-assembled during the phase separation of an unstable mixture, a process called spinodal decomposition (SD). In contrast, the shapes of a sample of spherical-type nanostructures from feather barbs of six species show a poor match to SD. However, spherical nanostructures show a strong morphological similarity to morphologies produced by phase separation of a metastable mixture, called nucleation and growth. We propose that colour-producing, intracellular, spongy medullary β-keratin nanostructures develop their characteristic sizes and shapes by phase separation during protein polymerization. We discuss the possible role of capillary flow through drying of medullary cells in the development of the hollow morphology of typical and spongy feather medullary cells.

Keywords: structural colour; self-assembly; β-keratin; coherent scattering; phase separation; spinodal decomposition

1. INTRODUCTION

Most organismal structural colours are produced by coherent scattering, or interference, of ambient light by nanostructures with periodic spatial variation in refractive index (Prum & Torres 2003). Here, coherent scattering means that the phase relationships among the scattered light waves determine the scattered light spectrum (Prum & Torres 2003). Coherent scattering includes constructive interference, diffraction, Bragg scattering and thin-film scattering. Coherent scattering can be contrasted with incoherent scattering—such as Rayleigh, Tyndall and Mie scattering—in which the phase relationships among the scattered waves are random (Prum & Torres 2003).

Although the great diversity of organismal nanostructures shares this common physical basis in dielectric spatial periodicity (Prum & Torres 2003; Vukusic & Sambles 2003; Prum *et al.* 2004), the nanostructures of different organisms vary tremendously in the organization and composition of this periodicity (Parker 1999; Srinivasarao 1999; Vukusic & Sambles 2003).

How do these colour-producing nanostructures develop? What physical and biological mechanisms do organisms use to construct arrays of quasi-ordered and highly periodic nanostructures? Surprisingly, these fundamental questions have been little studied. Research on the development of colour-producing biological nanostructures is critical for understanding

*Author and address for correspondence: Department of Ecology and Evolutionary Biology, Yale University, PO Box 208015, New Haven, CT 06520, USA (richard.prum@yale.edu).
†Present address: University of Missouri at Kansas City Medical School, Kansas City, MO 64108, USA.

One contribution of 13 to a Theme Supplement 'Iridescence: more than meets the eye'.

Received 28 November 2008
Accepted 6 January 2009

condition dependence in structurally coloured communication signals (Prum 2006). Condition dependence is predicted by some mechanisms of the evolution of signals used in social and intersexual communication (Andersson 1994).

A few studies indicate that colour-producing biological nanostructures develop by either complex mechanisms of cellular physiology and growth or more simple physical mechanisms of nanoscale self-assembly. A ground-breaking study by Ghiradella (1989) showed that the bicontinuous, colour-producing, air–chitin nanostructures in the green wing scales of the butterfly *Mitoura gryneus* develop from a prepattern formed by the complex, reticulate growth of smooth endoplasmic reticulum and cellular membrane into the central body of each balloon-shaped, wing-scale cell. Following establishment of the membrane prepattern, extracellular chitin is deposited into the lumen of these complex structures but outside the cell to create the optical nanostructure. After cell death, the remaining cytoplasmic spaces between the chitin become filled with air to create the refractive index difference that produces light scattering. Thus, internal nanostructures in insect scales illustrate some of the subtle distinctions between nanostructural self-assembly and cellular physiological assembly. Although chitin is a protein polymer formed by self-assembly of extracellular fibrils (Neville 1975, 1993), the nanoscale structure of chitin inside butterfly and weevil scales is created by a biological prepattern of membranes, which is probably determined by complex cellular physiology and growth, rather than self-assembly.

Structurally coloured butterfly scales are extremely variable, and not all optical butterfly nanostructures develop in the same way. Ghiradella (1974, 1989) has also shown that mechanical buckling of chitin is involved in the development of colour-producing superficial ridges of *Colias* butterfly wing scales.

Durrer & Villiger (1967) described the development of the hollow melanosomes that produce the structural colours in the feather barbules of a starling. The size of the central air cavity within each melanosome is determined by cellular mechanisms within melanocytes prior to transfer to the barbule keratinocyte.

In contrast to the highly regulated developmental mechanisms in butterfly scales and hollow avian melanosomes, Hemsley *et al.* (1994, 1996, 1998) have hypothesized that the exines of the cell wall spores and pollen grains of vascular plants consist of a self-assembled nanostructure of sporopollenin. Hemsley *et al.* (1994, 1996, 1998) focus on *Selaginella*, in which the exines may form an iridescent, biological opal of sporopollenin spheres in a hexagonal packing. In a series of biomimetic experiments, Hemsley *et al.* (1994, 1996, 1998) were able to simulate the development of very similar, complex nanostructures with the self-assembly of polymer colloids.

2. SPONGY MEDULLARY FEATHER KERATIN

The structural colours of avian feather barb rami are produced by β-keratin nanostructures in the medullary cells of the barb. These quasi-ordered, or amorphous, nanostructures function by coherently scattering light from their air–β-keratin interfaces (Prum 2006; Prum *et al.* 1998, 1999). Colour-producing intracellular β-keratin nanostructures have independently evolved many times and are known from over 20 different families of birds (Prum 2006). These spongy air and β-keratin nanostructures come in two distinct classes (figure 1; Dyck 1976; Prum 2006). 'Channel' nanostructures consist of β-keratin bars and air channels with elongate, tortuous and twisting forms (figure 1*a*,*b*). 'Spherical' nanostructures consist of highly uniform, spherical air cavities created by curved β-keratin bars of various thicknesses and frequently interconnected by tiny air passages (figure 1*c*,*d*).

Here, we investigate the development of the colour-producing, spongy, channel-type nanostructure in the blue feather barb rami of the blue-and-yellow macaw (*Ara ararauna*, Psittacidae; figure 2) using transmission electron microscopy (TEM). Auber (1971/1972) observed the development of colour-producing medullary barb cells using light microscopy, but his method did not allow him to describe the development of the colour-producing nanostructure itself because it is smaller than the wavelengths of visible light.

Our observations support the conclusion that these β-keratin nanostructures are self-assembled within medullary keratinocytes. To examine the mechanism of self-assembly further, we compared the shapes of spongy medullary nanostructures from bird species with channel-type ($n=9$) and spherical-type ($n=6$) bird feathers with experimental data from a polymer blend undergoing phase separation by *spinodal decomposition* (SD; Takenaka & Hashimoto 1992).

3. SELF-ASSEMBLY BY PHASE SEPARATION

Self-assembly is a ubiquitous phenomenon where molecular interactions and thermal fluctuations guide the formation of structures at the supermolecular, nano- and microscales (Jones 2002). We hypothesize that the sphere and channel nanostructures in medullary cells self-assemble during the phase separation of β-keratin from the remainder of the cytoplasm.

The stability of a mixture of two fluids depends on both the interactions between individual molecules and the concentrations of the components (Jones 2002). Entropy, embodied by random thermal fluctuations, typically favours the stability of a mixture. Repulsive interactions between dissimilar molecules favour the separation of the two molecular species into two distinct macroscopic phases. Vivid examples of this phenomenon can be found in the kitchen. To the pleasure and frustration of many, ethanol and water readily form stable mixtures, while oil and water in salad dressing separate when they are not vigorously mixed. The stability of a mixture can depend on the relative proportions of the fluids or other thermodynamic parameters, such as temperature.

The impact of the interplay between the entropy and molecular interactions on the stability of a mixture is embodied in a phase diagram (figure 3; Jones 2002). The mixture is stable when the repulsive molecular interactions between different molecules, measured by

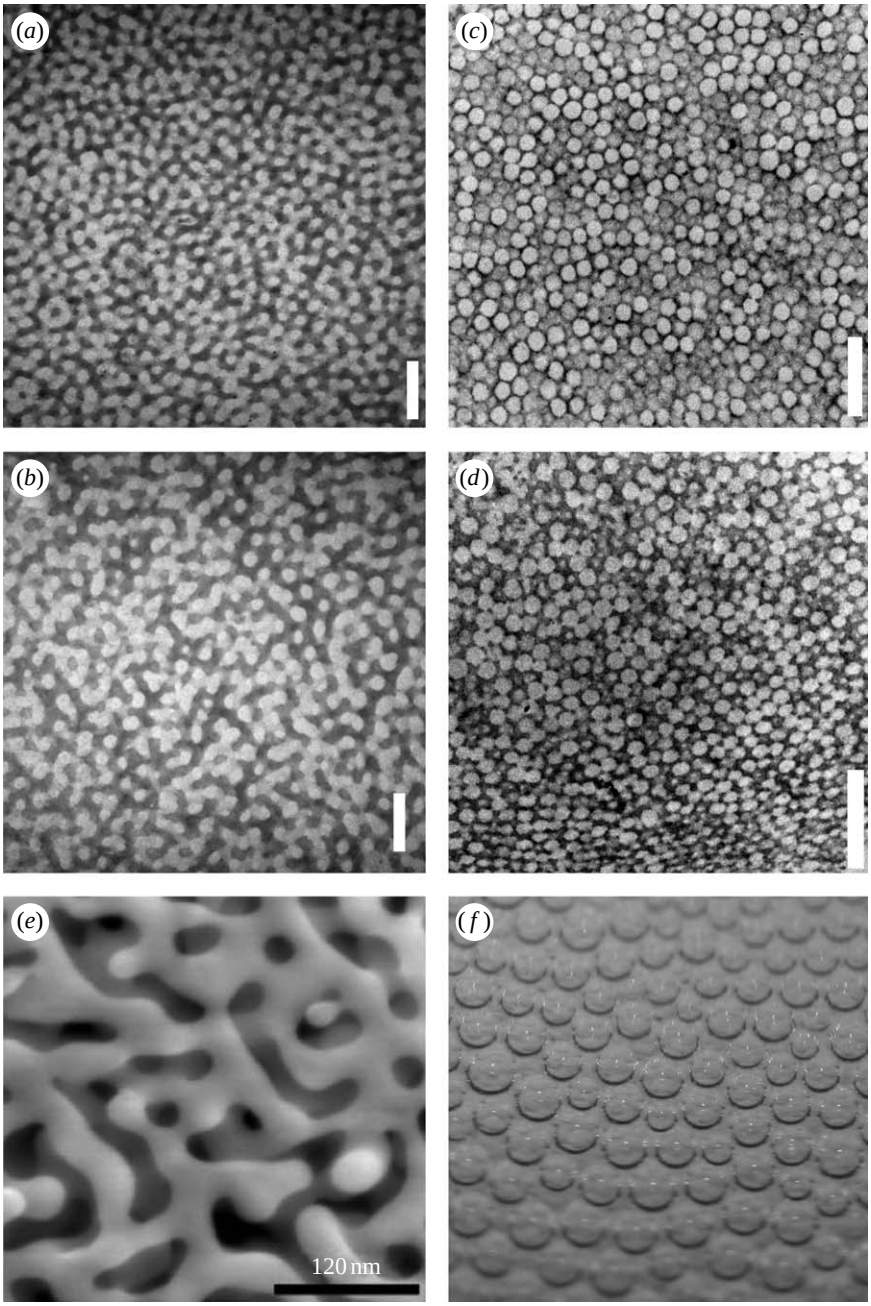

Figure 1. Transmission electron micrographs of colour-producing (*a*,*b*) channel-type and (*c*,*d*) sphere-type nanostructures from medullary cells of avian feather barb rami, and examples of phase separation by (*e*) spinodal decomposition (SD) and (*f*) nucleation and growth. (*a*) Black-capped kingfisher *Halcyon pileata* (Alcenidae, KU48795); (*b*) Asian fairy-bluebird *Irena puella* (Irenidae, KU101420); (*c*) blue-crowned manakin *Lepidothrix coronata* (Pipridae, KU87685); and (*d*) red-legged honeycreeper *Cyanerpes cyaneus* (Thraupidae, KU88256). The dark-staining material is β-keratin and the unstained voids are air. (*e*) Scanning electron microscopy image of nanoporous gold produced by SD of an Ag–Au alloy (from Erlebacher *et al.* 2001). (*f*) Carbon dioxide bubbles produced by a nucleation and growth phase separation in beer. Magnifications: (*a*) 30 000×, (*b*) 30 000×, (*c*) 20 000×, and (*d*) 25 000×. Scale bars: (*a–d*) 500 nm.

the parameter χ, are small compared with the random energy available from thermal fluctuations, measured by $k_B T$, where k_B is Boltzmann's constant and T is the absolute temperature. Below a critical value of $k_B T/\chi$, typically of the order of 1, the stability of a mixture depends on its composition, the proportions of the two fluids. In figure 3, ϕ indicates the volume fraction of one molecule in the mixture. For example, $\phi = 0$ or 1 would be a pure sample of molecule A or B, while $\phi = 0.5$ would be a one-to-one mixture of A and B. While systems consisting almost entirely of one molecular species remain stable, systems with intermediate compositions will unmix or phase separate into two stable compositions. Mixtures will be stable at all compositions above the phase-separation boundary (figure 3, solid line), but will phase separate below that line.

The mechanism by which phase separation proceeds depends on the stability of the system to small fluctuations in composition. When there is no activation barrier to separation, a mixture is unstable and phase separation occurs through a relatively smooth and well-characterized process called SD. When an

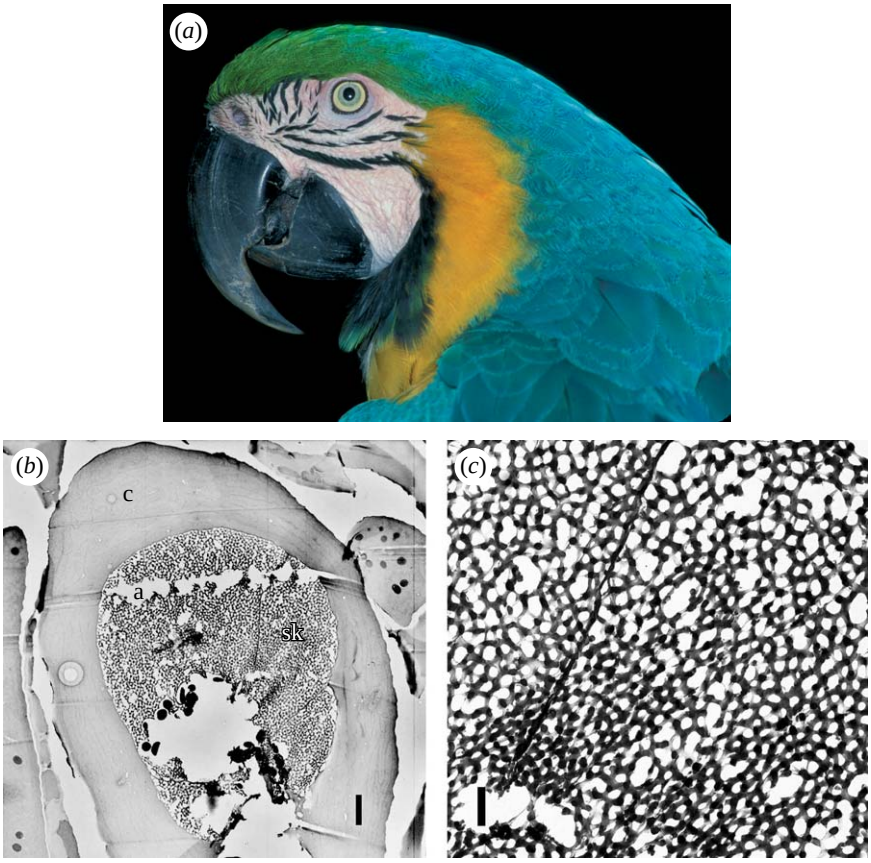

Figure 2. (*a*) Adult blue-and-yellow macaw (*A. ararauna*) (photo by T. Laman, VIREO, with permission). (*b*) TEM image of a single barb ramus showing the solid β-keratin cortex and the spongy medullary β-keratin. The rip in the section (a) is an artefact. (*c*) TEM image of the channel-type spongy medullary β-keratin. The solid line running through the image is the cell membrane boundary between two neighbouring medullary cells. Scale bars: (*b*) 2 μm and (*c*) 500 nm. a, sectioning artefact; c, cortex; sk, spongy medullary keratin.

activation energy barrier stabilizes the system against demixing, a mixture is metastable and will not phase separate unless it is 'seeded' with an initial particle composed of the minority phase that is above a critical size (Jones 2002). This mechanism of phase separation is called *nucleation and growth*. Nucleation can occur by random thermal fluctuations or by interactions with edges or impurities (Jones 2002). In figure 3, the solid line, called the *binodal line*, marks the boundary between mixed and phase-separated systems. Just below the binodal, mixtures separate via nucleation and growth. Below the dashed *spinodal line*, systems unmix by SD (figure 3).

Systems unmixing by SD display a characteristic sponge-like structure of interconnected channels of the two phases (figures 1*e* and 3). While the specific structure in each region of a phase-separating sample is different in every instance, the overall structure of SD is universal. The structures formed during nucleation and growth are more diverse. For simple fluids, they typically consist of isolated spherical droplets of the minority phase that grow over time (figure 1*f*). The droplet size distribution depends strongly on the kinetics. If nucleation is fast and growth is slow, droplets are nearly identical or 'monodisperse', otherwise they can be of very different sizes or 'polydisperse'. When the droplets are well separated, the overall structure of the material is completely random, but, as they get close to one another, the droplet positions can become correlated and even form periodic structures (Hemsley *et al.* 1994, 1996, 1998).

The morphologies produced by these two modes of phase separation are strikingly similar to the channel and sphere classes of β-keratin nanostructures (figure 1*e*,*f*). In this paper, we make a quantitative comparison of avian nanostructures with experimental data on the SD of a polymer blend. Finding good correspondence, we hypothesize that the characteristic forms of these biological nanostructures develop by phase separation.

4. METHODS

4.1. Feather sampling and microscopy

We examined growing feather germs, or pin feathers, from the back and crown of an adult male blue-and-yellow macaw (*A. ararauna*). Feather germs were 2–4 cm in length at the time they were sampled. Each feather germ was fixed and stored in Karnovsky's fixative (2.5% glutaraldehyde and 2.5% paraformaldehyde), and embedded in plastic for transmission electron microscopy.

Pennaceous feather structure grows by a complex mechanism of helical growth within the tubular feather germ (Lucas & Stettenheim 1972; Prum 1999; Prum & Williamson 2001). Feather growth involves three different maturation gradients. The primary distal–proximal gradient involves maturation of feather cells

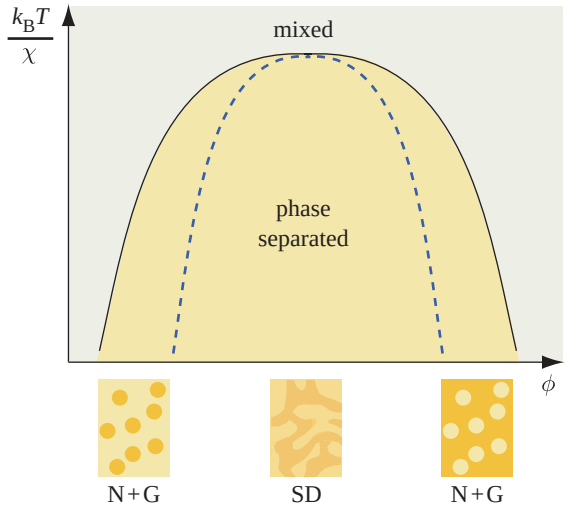

Figure 3. A schematic phase diagram showing the relationship between the temperature (k_BT/χ), composition (ϕ) and the stability of a mixture. k_B is Boltzmann's constant, T is the absolute temperature and χ is the strength of interactions between dissimilar molecules. In feathers, ϕ would represent the volume fraction of β-keratin. At high-temperature conditions, a molecular mixture will be stable at any composition, but below the phase-separation boundary (solid line) the solution will phase separate. Mixtures below the spinodal line (dashed line) are unstable, and will phase separate by SD, which produces bicontinuous channels of each material (middle inset). Mixtures between the spinodal line and the phase boundary are metastable, and will only phase separate through nucleation and growth (N+G), which produces spherical shapes (left and right insets).

as they emerge from the feather follicle out of the skin. Distal cells are older and more mature than proximal cells. Within a single horizontal section of a feather germ, a second ventral–dorsal gradient involves increasing maturation of barb ridge cells as barb ridges grow helically around the tubular feather germ, towards the dorsal surface of the tubular feather germ, to fuse to the rachis. Third, within a single barb ridge, cell maturation progresses along a superficial–internal gradient; more superficial barbule plate cells mature before the more internal, or basal, cells of the barb ramus, which is the shaft of the barb.

Because we cannot follow individual cells as they mature, we documented barb ramus cell maturation and keratin self-assembly by tracking homologous medullary cells within multiple barb ridges along the various maturation gradients. Thus, thin sections of embedded feather germs were made at different distances from the base of the germ (between 1 and 8.25 mm) and different radial positions around the tubular feather germ (between 60° and 30° from the dorsal midline). Medullary cells were completely mature at 10 mm from the base of the feather germ.

Thin sections were viewed with a JEOL EXII transmission electron microscope, and images were digitally captured using a Soft-Imaging Megaview II CCD camera (1024×1200 pixels).

The development of a series of homologous spongy medullary cells is described by following barb ridges at two radial positions (60° and 120° from the rachis) along the proximal–distal maturation gradient from the base of the growing feather germ within the follicle and the completely mature barb cells. The distances in millimetres were measured from the base of the developing feather germ, and are a proxy of cell age and developmental stage.

4.2. Comparative structural analysis

To test the SD hypothesis for self-assembly of spongy medullary β-keratin, we analysed transmission electron micrographs (TEMs) of mature spongy medullary keratin of 15 species from 12 different families of birds. The species were identified as nine spherical-type and six channel-type nanostructures based on visual observation of the nanostructures.

To quantify these structures, we estimate the static structure factor, $S(k)$, from TEM images. The static structure factor can be directly measured with an appropriate scattering method, such as light scattering or neutron scattering. It is essentially a diffraction pattern of a wave passing through the sample. We estimated $S(k)$ by calculating the azimuthal average of the Fourier power spectrum of TEM images in MATLAB. This method is identical to the 'radial' averages of the Fourier power spectrum calculated by Prum & Torres (2003). A peak in $S(k)$ corresponds to the predominant variation in the image contrast at a wavelength inversely proportional to the value of k_{max}, the wavevector or spatial frequency at the peak. For comparison across species, which have different characteristic length scales and different strengths of contrast, we normalized all values of k by k_{max} and all values of $S(k)$ by $S(k_{max})$. The normalized plots of $S(k)$ for channel and spherical classes of nanostructure were compared with analogous light scattering data from a spinodally decomposing polymer mixture of polybutadiene and polyisoprene (Takenaka & Hashimoto 1992).

5. RESULTS

5.1. Medullary cell and nanostructure development

At 1.5 mm above the base of the feather germ, distinct barb ridges are well organized (figure 4*a*,*b*). The peripheral barbule plate cells are well differentiated and linearly organized into presumptive barbules, but the medullary cells in the more basal (i.e. internal) positions within the barb ridge are small and poorly differentiated. In TEMs, the medullary cells are weakly attached to one another, and separated by gaps (figure 4*b*). These gaps may be artefacts of sectioning for TEM, but similar spaces were observed by Matulionis (1970) and Alibardi (2005) in chick embryos. No keratinization is occurring, but melanosomes are being transferred from melanocytes into medullary keratinocytes. Melanocyte processes, and occasionally entire melanocytes, migrate amidst the medullary cells within the barb ridge (figure 4*a*). This may be facilitated by the gaps between medullary cells at this early stage.

At 3 mm, medullary cells exhibit greater organization and fewer gaps between cells (figure 4*c*).

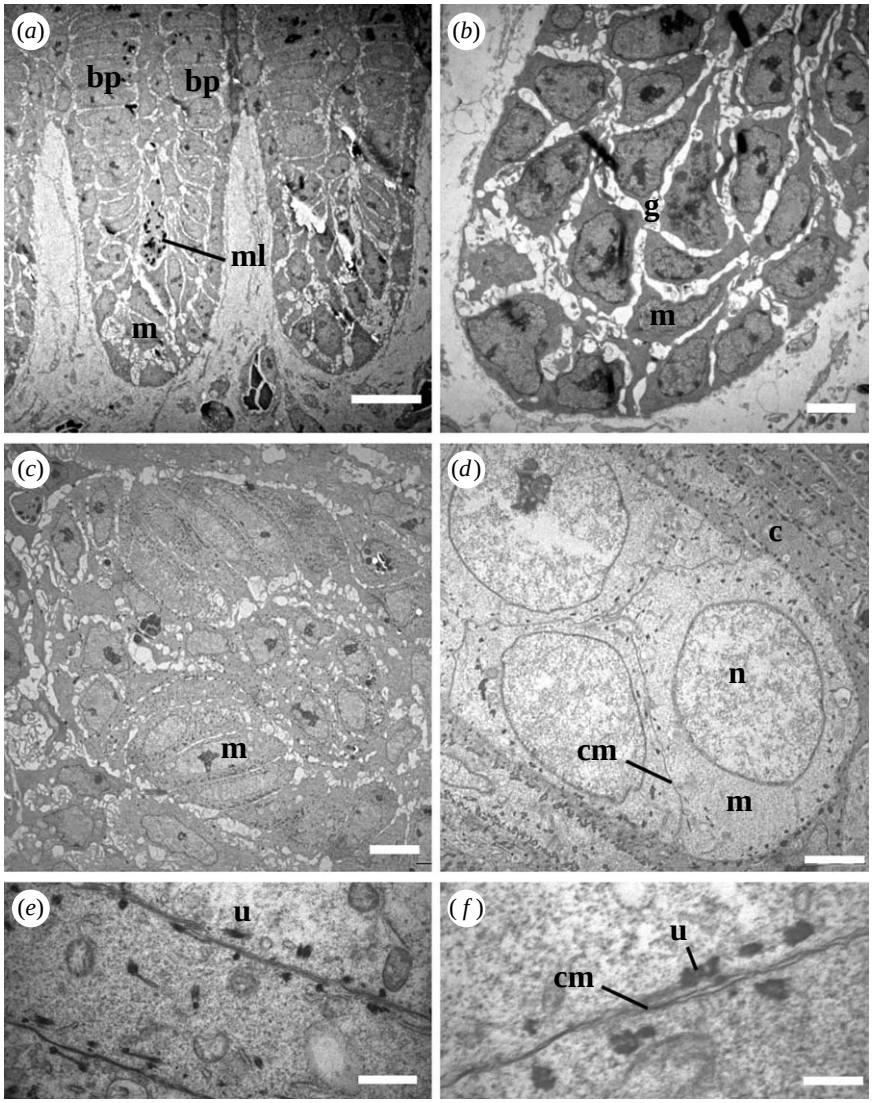

Figure 4. Early stage of medullary cell development. (*a*) Separate barb ridges with differentiated barbule plates, weakly organized medullary cells and an occasional melanocyte. (*b*) Medullary cells are poorly differentiated, weakly interconnected and separated by gaps. (*c*) Medullary cells elongate and more closely connected with fewer gaps. (*d*) Medullary cells expand to their mature size and boxy shape with enlarged nucleus. (*e*,*f*) Cell membranes between medullary cells with unknown dark-staining structures. Distances from the base of the feather germ: (*a*,*b*) 1.5 mm, (*c*,*d*) 4 mm, (*e*,*f*) 5 mm. Scale bars: (*a*) 10 µm, (*b*) 3 µm, (*c*) 4 µm, (*d*) 2 µm, (*e*) 1 µm and (*f*) 300 nm. bp, barbule plate; c, cortical cell; cm, cell membrane; g, intercellular gap; m, medullary cell; ml, melanocyte; n, nucleus; u, unknown structure.

At 4–5 mm, the medullary cells have increased to their mature size and realized their final shapes, and neighbour boundaries (figure 4*d*). Neighbouring cells have well-defined cell membranes bordering one another, and cells do not separate during TEM fixation and sectioning. Cell nuclei are large and less densely staining. Many cells have unidentified darkly staining structures that are approximately 200 nm by 100 nm that occur within 100 nm of the cell membrane (figure 4*d*–*f*).

Starting at 4–5 mm, the medullary cells begin to develop large 'transparent' or 'clear' (i.e. electron-lucent) regions, which expand in size to occupy the majority of the volume of the cell (figure 5*a*–*d*). Our observations indicate that these clear regions are cytoplasmic 'voids' that lack most of the larger, electron-dense biological structures. These voids begin as one or a few small clear regions in the centre, which unite as they expand into a single large void (figures 5 and 6). As the voids expand, the nuclei, melanosomes and other observable cellular structures become restricted to the extreme margins of the cell (figure 6*a*,*b*). These expanding voids do not appear to be membrane bound or created by cytoskeletal filaments; rather, they are bounded by a line of dark material that appears to be accumulated intracellular contents that have aggregated at the expanding edge of the void (figure 5*c*,*d*).

Starting at 5.5–6 mm, the medullary cells begin to keratinize along their membrane boundaries with neighbouring cells (figure 5*e*,*f*). This initial peripheral keratinization creates interconnected linear keratin processes that are tens of nanometres to more than 100 nm wide and up to 1 µm in length. These processes occasionally branch, or bifurcate, at very small angles (less than 30°) to create an anastamosing matt of branches. In cross section, these keratin processes appear as darkly staining circular bodies near the cell membrane. At this stage, they closely resemble the

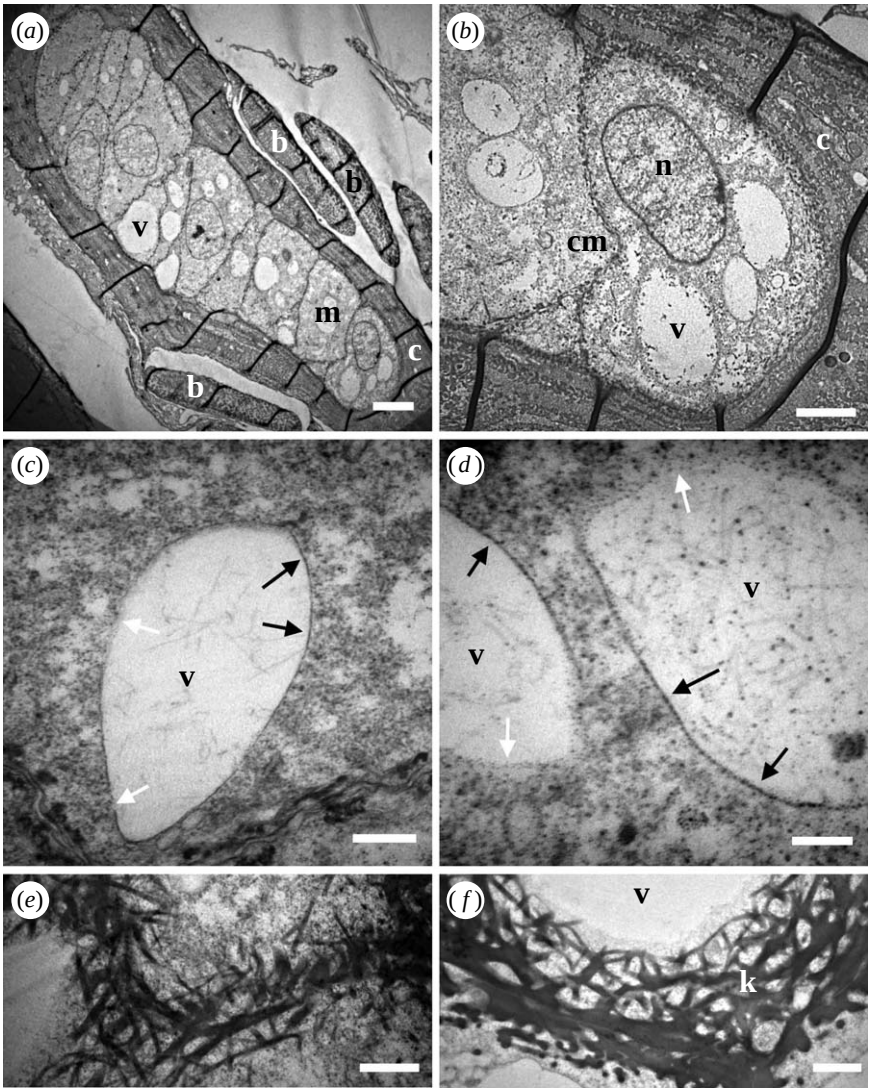

Figure 5. Intermediate stage of medullary cell development. (*a*) Medullary cells expand to their full mature sizes with closely adhering cell membranes. Clear, electron-lucent cytoplasmic voids begin to appear. (*b*) Medullary cell with expanding cytoplasmic voids that lack most electron-dense structures. (*c*,*d*) Cytoplasmic voids showing little material within them. The margins of the voids are sometimes marked by aggregated materials (black arrows), but in other places they clearly lack a surrounding membrane (white arrows). Some dark speckling in (*d*) is a staining artefact. (*e*,*f*) Peripheral β-keratin structures that radiate from the cell membranes into neighbouring cells. Distances from the base of the feather germ: (*a*–*d*) 5 mm, (*e*) 6 mm, and (*f*) 7.5 mm. Scale bars: (*a*) 5 µm, (*b*) 2 µm, (*c*) 400 nm, (*d*) 200 nm, and (*e*,*f*) 1 µm. b, barbule; c, cortical cell; cm, cell membrane; k, β-keratin; m, medullary cell; v, cytoplasmic voids.

initial keratinized structures of the non-spongy barbule and ramus cortical cells (figure 6*a*,*b*). These initial linear keratin processes do not extend into the centre of the cell; rather, they radiate at low angles that are nearly parallel to the cell membrane. In TEM sections of the end of a medullary cell, the linear processes show a tangled 'crown of thorns' form (figure 5*e*,*f*). At their peak extent, these peripheral β-keratin structures extend further from the cell membrane than the width of the β-keratin along the cell membrane in final mature cells (figures 2*c* and 5*e*,*f*). This implies that these β-keratin structures are either compacted or remodelled during later development.

By 7 mm, every medullary cell appears as a single, large, entirely empty transparent void (white areas in figure 6*a*,*b*). Nuclei, melanosomes and other organelles are restricted to the extreme margins of the cells. The peripheral keratin now forms a solid layer approximately 750 nm thick. Although the medullary cells look empty, subsequent development demonstrates that these featureless cells are indeed living.

After 7 mm, clouds of patchy grey (i.e. electron-dense) material begin to appear at the periphery of the clear voids within each cell (figure 6*c*,*d*). This material appears to have expanded from the periphery of the cells back into the cytoplasmic voids towards the centre of the cell. Keratinization of the spongy medullary matrix then proceeds by broad regional precipitation of a characteristic spongy pattern of keratin channels out of this amorphous granular cytoplasmic material.

Relatively few cells were observed in the intermediate stages of this process (figure 7), implying that it proceeds rapidly, perhaps even within a few hours. Commonly, TEMs show neighbouring cells in substantially different stages of keratinization. Early stages of spongy keratin polymerization are characterized by the appearance of a few keratin rods within a local region

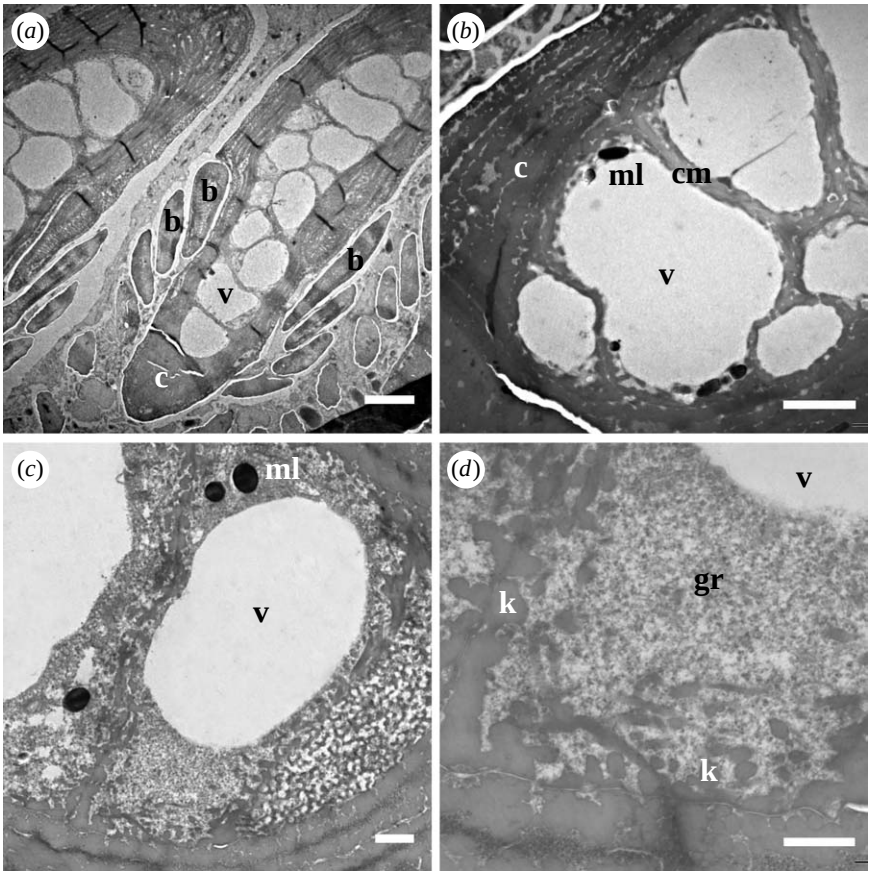

Figure 6. Late intermediate stage of medullary cell development. (*a*) Barb ridge with all medullary cells occupied by a single, large cytoplasmic void. (*b*) Medullary cells with fully expanded central void (v). Melanosomes and nuclei are restricted to the extreme margins of each cell, and the peripheral β-keratin along the cell membrane has been compacted or remodelled. (*c*,*d*) A cytoplasmic void begins to shrink with the expansion of granular electron-dense material from the margins of the cell. Distances from the base of the feather germ: (*a*–*d*) 7.5 mm. Scale bars: (*a*) 5 µm, (*b*) 3 µm, (*c*) 1 µm, and (*d*) 600 nm. b, barbule; c, cortical cell; cm, cell membrane; gr, granular material; m, medullary cell; ml, melanosome; v, cytoplasmic void.

(approx. 500 nm^2) of granular cytoplasmic material. Other images later in the process show a more complete nanostructure that is still vague and unresolved in specific places (figure 7*a*–*c*). Cytoplasmic spaces among developing keratinized bars are occupied by granular, electron-dense materials including ribosomes and possibly other organelles (figure 7*a*,*b*). Importantly, during spongy keratinogenesis, there are no indications of cellular intermediate filaments, microtubules, endoplasmic reticulum, cell membrane, etc. to organize the spatial nanoscale patterning. Rather, the pattern arises by self-assembly from within regions of granular cellular cytoplasmic materials.

As spongy keratinogenesis proceeds, the clear voids are greatly reduced in size and increasingly restricted towards the centre and basal regions of each medullary cell (figure 7*d*). Melanin granules become surrounded by and incorporated within the basal region of the spongy keratin (figure 7*d*,*f*). Nuclei and other organelles are progressively restricted to the basal regions of each cell towards the centres of the multicellular barb ramus (figure 7*d*).

When the medullary cells completely dehydrate and die, the cytoplasmic spaces within the spongy nanostructure, the remaining cytoplasmic voids and the nuclear envelope become filled with air, creating the dielectric, quasi-ordered, photonic nanostructure that is responsible for vivid structural colour production in the mature plumage of the bird. Mature blue feather barb rami from blue-and-yellow macaw (*A. ararauna*) show expansive regions of channel-type spongy medullary keratin, melanin granules distributed in intermediate positions and larger, basally distributed air-filled spaces (figure 2*b*,*c*). These large air-filled spaces were clearly occupied by cellular nuclei and the remaining cytoplasmic voids of the cells when they died. Further evidence of remodelling or compression of the initial, peripheral β-keratin structures comes from the very narrow (30–50 nm) continuous keratin volume marking the position of the membrane junctions between neighbouring cells (figure 2*c*).

5.2. Test of the spinodal decomposition hypothesis

The SD mechanism of phase separation produces highly characteristic, scale-invariant morphologies, or shapes, of the two bicontinuous separating materials. Regardless of size, the spinodal morphology will produce the same spatial relationships between the regions of the two materials—here, β-keratin and cellular cytoplasm. To examine the hypothesis that the channel-type β-keratin nanostructures in avian feather barb rami self-assemble by SD, we compared the scale-independent

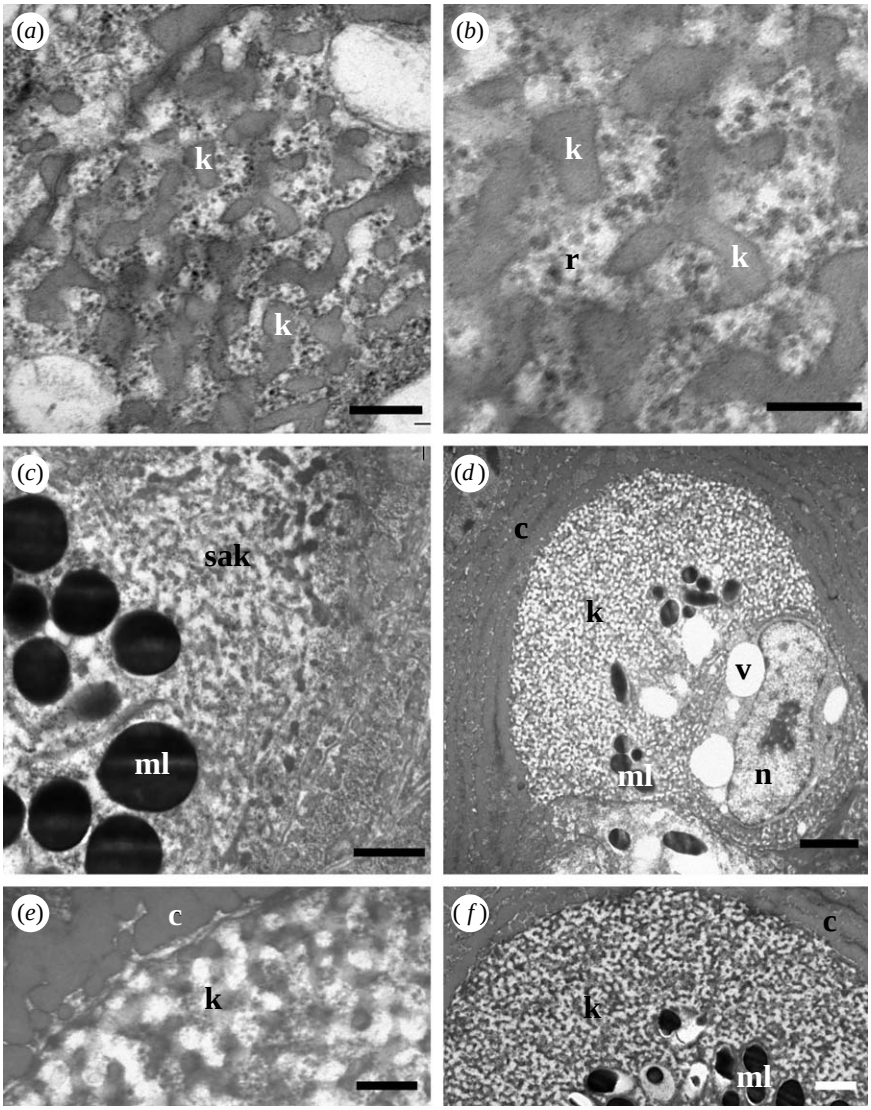

Figure 7. Development of spongy medullary feather β-keratin. (*a*,*b*) Emergence of curved bars of spongy β-keratin within granular electron-dense materials including ribosomes. (*c*) Region of self-assembling β-keratin above an aggregation of melanosomes. (*d*) Medullary cell with extensive spongy β-keratin peripheral to an array of melanosomes. Cytoplasmic voids are greatly reduced and the nucleus is visible again. Keratin between the voids and the melanosomes is not completely assembled. (*e*,*f*) Mature spongy β-keratin in final stages of assembly. Distances from the base of the feather germ: (*a*–*f*) 7.5 mm. Scale bars: (*a*,*e*) 300 nm, (*b*) 200 nm, (*c*) 600 nm, (*d*) 2 µm, and (*f*) 1 µm. b, barbule cell; c, cortical cell; k, spongy β-keratin; ml, melanosome; n, nucleus; r, ribosome; sak, self-assembling keratin; v, cytoplasmic void.

distribution of different spatial frequencies of variation in composition of spongy β-keratin nanostructures with observations of light scattering by polymer blends in SD (Takenaka & Hashimoto 1992).

First, we compared the shapes of the frequency distributions of spatial frequencies in β-keratin–air composition (calculated from Fourier transforms of TEMs) of mature channel-type nanostructures from nine avian species with measurements of the spinodally decomposing polymer mixture (figure 8*a*). The normalized spatial frequencies from the feather data provide a very accurate fit to the observed SD observation at higher spatial frequencies (figure 8*b*). There is substantial variation at lower spatial frequencies, but these are probably produced by large-size-scale artefacts in the TEM images, such as large-scale variations in image darkness and finite sample effects. In contrast, spatial frequency profiles from spongy medullary keratin of sphere-type nanostructures from six different birds species all show a second peak at higher spatial frequencies (between 1.6 and 2 $k/k_{\max}$), which is absent from the SD data, and often a strikingly narrower peak in spatial frequency.

These data support the conclusion that channel-type keratin nanostructures are self-assembled by a SD process. As expected from their qualitative morphology, these data also indicate that sphere-type nanostructures deviate substantially in shape from the expectations of the SD mechanism.

6. DISCUSSION

Nearly a century ago, Thompson (1917) responded to the growing adaptationist trend in comparative, functional and evolutionary biology by arguing powerfully that physical and chemical forces have a fundamental role in the development of organismal form. Since that time, Thompson's 'structuralist' approach

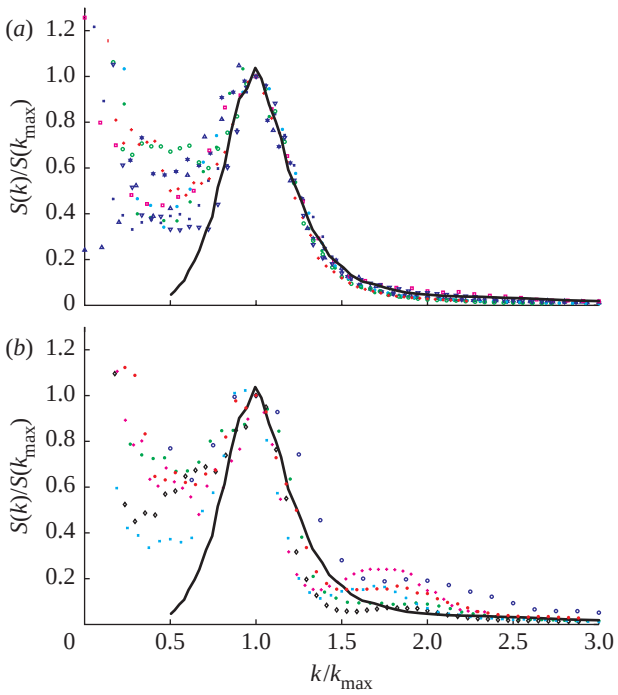

Figure 8. Normalized spectra of the spatial frequencies of variation in composition of mature spongy medullary feather keratin TEMs (coloured data points) and a polymer mix in SD (solid line; from Takenaka & Hashimoto 1992). (*a*) Nine species of channel-type nanostructures show strong congruence with SD at higher spatial frequencies above the peak. (*b*) Six species of sphere-type nanostructure show variation in the breadth of the peak and a distinct secondary peak at higher spatial frequencies (approx. 1.6–2 k/k_{max}). (*a*) Channel-type species sampled: *Porphyrio martinica* (Rallidae); *Motmotus motmota* (Motmotidae); *Ifrita kowaldi* (Cinclosomatidae); *I. puella* (Irenidae); *Vireolanius pulchellus* (Vireonidae); *Cyanocorax yncas*; *Cyanocorax beecheii* (Corvidae); *Muscicapa turquosa*; and *Sialia sialis* (Turdidae). (*b*) Sphere-type species sampled: *Cotinga cayana* (Cotingidae); *Lepidothrix serena*; *L. suavissima*; *L. coronata* (Pipridae); *Tangara seledon*; and *C. cyaneus* (Thraupidae).

has often been eclipsed by the adaptationist perspective in evolutionary and developmental biology (Gould & Lewontin 1979; Wake 1991; Amundson 2001, 2005). Thus, although no modern biologists would deny the role of physical and chemical forces in the development and evolution organismal form, research directly on these processes is still rather rare. As proposed by Hemsley and colleagues (Hemsley *et al.* 1994, 1996, 1998; Hemsley & Griffiths 2000), this research is a nanoscale exploration of Thompson's hypothesis concerning abiotic physical forces in developmental biology. Here, we examine whether crucial details of the development of colour-producing β-keratin nanostructures in bird feathers may be described by two physical mechanisms of soft-condensed-matter physics—specifically, capillary flow in drying suspensions, and phase separation.

6.1. Capillary flow in a drying cell

TEMs of spongy medullary keratin development indicate that a complex sequence of cellular physiological events establishes unusual cellular conditions preceding spongy nanostructure self-assembly—the development of large, clear intracellular voids. The TEMs indicate that the materials within the cytoplasm are moving towards the periphery of the cell, producing an expanding central region that is devoid of larger biological structures or electron-dense materials (figures 5 and 6). Using light microscopy, Auber (1971/1972) observed the development of clear areas within spongy medullary cells. Matulionis (1970) described these structures in embryonic chick barb rami using TEM. Careful examination of the edges of the voids indicates that they are not membrane-bound vacuoles, as hypothesized by Matulionis (1970) and Alibardi (2002, 2005). Rather, the margin of each void appears to be defined by the accumulation of cellular materials, similar to flotsam washed up on a beach (figure 5*c*,*d*). The cells are still living at this stage; ribosomes, the nucleus and melanosomes will all reappear at later stages of development (figure 7*d*). Interestingly, mature medullary cells from feather barbs and rachis have a large hollow volume at the centre, which apparently develops by this mechanism (see below; Lucas & Stettenheim 1972).

We propose that this cytoplasmic void is formed by capillary flow as the cells begin to dry. This same process produces ring stains in drying drops of coffee or red wine (Deegan *et al.* 1997; Tsapis *et al.* 2005). Evaporation from the surfaces of a drying drop of liquid will produce capillary flow towards the 'pinned' edges of the drop, which cannot retract as the drop loses volume because of strong capillary attractions to the material at the surface. Owing to the constraint on shrinking the edges of the droplet, fluid will travel towards the drying edges to compensate for the evaporative loss, creating a flow or net evaporative flux (Deegan *et al.* 1997). This capillary flow will transport dispersed materials (solutes) towards the pinned edges of the drop, resulting in a ring-shaped stain of deposited materials around the edges of a drying drop. Originally described in drying droplets on a two-dimensional surface (Deegan *et al.* 1997), the phenomenon is known to form shells in drying three-dimensional droplets of polymer colloids (Tsapis *et al.* 2005).

We propose that drying in the medullary keratinocytes creates capillary flow towards the margins of the cells, and forms a volume of cytoplasm at the centre of the cell that is devoid of larger molecules and organelles. The two requirements of this process—drying and pinned edges—are both met in these cells. Drying is a fundamental part of the keratinocyte maturation. All feather keratinocytes achieve their mature functions when they are dead and dry. Peripheral keratinization at the cell boundaries that precedes void formation would simultaneously (i) cut off the cytoplasm of each cell from diffusion of water from the dermal pulp of the feather germ, and (ii) structurally constrain the cell from shrinking in volume as it dries.

The capillary flow hypothesis raises the question of why the flow of cellular materials to the margins ceases and granular materials reappear and expand from the margins of the cells. The magnitude of capillary flow depends on the rate of drying. We hypothesize that a slowing of the rate of drying reduces capillary flow and

provides opportunity for cytoplasmic materials to diffuse back into the cytoplasm, creating the conditions that immediately precede the self-assembly of the spongy medullary keratin.

6.2. Self-assembly

Our TEM observations of development of colour-producing, spongy medullary feather keratin indicate that these nanostructures are self-assembled. The morphologies of the spherical- and spongy-type nanostructures closely match the morphologies produced by two distinct processes of nanoscale self-assembly by phase separation—SD and nucleation and growth. There is no evidence within these feather cells of a biological prepatterning mechanism of intermediate filaments, cell membrane, endoplasmic reticulum or other structural precursors to the nanostructure. Rather, the nanostructure emerges with its own intrinsic and characteristic form. Similarly, Matulionis (1970) was unable to identify any intermediate filament precursors to feather keratin.

Keratinization in the medullary cells begins peripherally near the cell membrane as in other feather keratinocytes of the barb cortex and barbules. Apparently, the expansion of the cytoplasmic voids disrupts the continuation of this process, and establishes the conditions for subsequent spongy nanostructure self-assembly. It is clear that the development of traditional solid β-keratin and the spongy medullary β-keratin are very distinct processes. Interestingly, there may be a role for some structural, cellular prepattern in the initiation of the peripheral keratin. The initial peripheral keratin bars radiate at low angles away from sites along the cell membrane.

6.3. Phase-separation kinetics

The role of phase separation in β-keratin self-assembly was suggested by the striking similarities of the stereotyped morphologies produced by the two fundamental mechanisms of phase separation—SD and nucleation and growth (figure 1*e*,*f*)—and the physical process of β-keratin self-assembly (Brush 1983).

Images of SD in well-characterized physical systems show a striking congruence with channel-type β-keratin nanostructures in bird feather barbs (figure 1*a*,*b*,*e*). Furthermore, the sphere-type spongy keratin nanostructures show strong resemblance to the spherical morphologies produced by nucleation and growth phase separation in metastable mixtures (figure 1*c*,*d*,*f*). Although the two fundamental classes of spongy keratin nanostructure were recognized over 30 years ago (Dyck 1976, 1978; Prum *et al.* 1999; Prum 2006), the phase-separation hypothesis provides the first explanation of (i) why there are two distinct classes of nanostructure, and (ii) why they have the specific shapes.

Our analysis of the size-independent variation in the shapes of spongy keratin nanostructures documents strong congruence between the structure factor (or the form of spatial variation) of a mixture in SD and a broad sample of channel-type feather nanostructures from nine different species (figure 8*a*). Substantial variations among datasets at small spatial frequencies were a consequence of large-scale deviations in image contrast and edge effects. By contrast, shapes of sphere-type nanostructures show distinct deviations from the shape of spinodal materials at higher spatial frequencies (figure 8*b*). The additional peak in $S(k)$ for these systems is characteristic of dense collections of spheres, which can be produced by nucleation and growth.

Heterogeneity within each cell in those factors that influence kinetic interactions of β-keratin and the cytoplasm (i.e. rate of drying, protein concentration, etc.) will create additional spatio-temporal patterning. For example, the wavefront of phase separation that appears to move through the cell volume is not accounted for by a simple description of SD.

SD produces a characteristic shape that expands in size and scale over time (Jones 2002). However, in experiments on phase-separating colloids, this characteristic shape expansion breaks down when the structures become large enough for gravity, or other external forces, to perturb the purely intermolecular interactions in the mixture (Aarts & Lekkerkerker 2004). Consequently, in order for β-keratin nanostructures to produce the appropriate species- and sex-specific structural colour when the feather cells are mature, the expansion of the spinodal spatial pattern must be halted and solidified (or 'quenched') at the appropriate size. Although phase separation provides a powerful explanation of the development of the *shape* of these β-keratin nanostructures, it raises a new question about the physical determination of nanostructure *size*, which is of critical importance to the ultimate communication function of these nanostructures in the lives of birds. We expect that the coupling of phase separation and the irreversible polymerization of β-keratin (Brush 1983) halts the phase-separation process and that competition between the rates of phase separation and polymerization selects the ultimate feature size of the nanostructures.

In conclusion, we propose that spongy medullary keratin nanostructures develop by phase separation of the intracellular mixture of β-keratin and cytoplasm. The channel-type nanostructures develop by spinodal composition of unstable mixtures, and sphere-type nanostructures develop by nucleation and growth of metastable mixtures. We further propose that self-assembly of spongy medullary keratin can be reproduced and studied *in vitro*. Our results extend Hemsley's hypothesis (Hemsley *et al.* 1994, 1996, 1998; Hemsley & Griffiths 2000) of nanoscale self-assembly from plant spore development to vertebrate integumentary appendages.

6.4. Evolution of spongy feather nanostructures

Our observations provide new insights into the evolution of colour-producing spongy medullary barb nanostructures. Medullary cells of the feather rami and rachis are identified by their large size, boxy shape and the central, air-filled space (e.g. Lucas & Stettenheim 1972). Air-filled medullary cells function to provide mechanical support to the rami and rachis of the feather, and are thus critical for the maintenance of

a planar vane that is critical to avian flight and many other feather functions. It is well understood that a hollow structure can provide more structural integrity for the same volume of material (Vogel 2003). Hollow feather medullary cells have convergently evolved with hollow plant sclerenchyma cells through selection for their mechanical properties (Niklas 1992).

Birds have apparently evolved to use the physical mechanism of capillary flow during drying to create the hollow, mechanically advantageous morphology of their medullary feather cells. This novel developmental mechanism also apparently created the opportunity for subsequent establishment of appropriate conditions for phase separation of β-keratin and cytoplasm within the cell. Apparently, these conditions are not created in solid cortical and barbule cells in which keratinization proceeds continuously from the periphery to fill the cell volume (Matulionis 1970). Colour-producing spongy keratin has never evolved in any other type of feather cell (Prum 2006).

Thus, colour-producing spongy keratin evolved through the co-option and specialization of mechanisms of development of hollow medullary cells that initially evolved to provide mechanical integrity to feather barbs and rachis. Many lineages of birds have independently evolved to exploit phase-separation mechanisms within medullary cells to create optical nanostructures out of β-keratin. The parallel evolution of precisely similar nanostructures in so many different lineages of birds indicates that the parameters necessary to produce dynamic phase separation during keratinogenesis are easily achieved and easily evolved in medullary keratinocytes.

6.5. Self-assembly and condition dependence

Some mechanisms of sexual selection predict that female preferences will evolve through natural selection to prefer male traits that honestly communicate mate quality or condition (Andersson 1994). Signal honesty is hypothesized to be reinforced by either dependence on a limiting nutrient (e.g. dietary carotenoids) or a substantial, physiologically costly investment.

In general, the self-assembly process does not require either limiting nutrients or extensive physiological investment, as hypothesized by condition-dependent sexual selection models. During development, spongy medullary cells establish the initial conditions for self-assembly of the colour-producing nanostructure through β-keratin synthesis and drying. By relying on predictable physical forces to construct the nanostructure, medullary cells eliminate many potential physiological mechanisms to mediate condition dependence during development. Furthermore, the additional amounts of β-keratin forming the actual bars within the spongy matrix are a trivial additional physiological investment compared with the volume of keratin in the entire feather.

Undisturbed phase separation results in the complete separation of the two materials (e.g. oil and water). We are not sure what causes the phase-separation process in spongy medullary cells to halt at the specific size scale appropriate to produce the colour required for that cell. But the self-assembly mechanism implies that it may be the irreversible polymerization of β-keratin that arrests the phase-separation process. Thus, the size scales of the spongy nanostructure, which determine the colour produced, may be controlled by the kinetic properties of the specific β-keratin molecules expressed in late medullary development. Little is known about the variation in molecular structure and kinetics of the β-keratins found in bird feathers and nothing is known specifically about the β-keratins expressed in spongy medullary cells (Brush 1978, 1993).

Another way to assess mechanisms of variation in structural coloration is to examine variation within a plumage. For example, microscopic observation of these structurally coloured bird feathers indicates that the process is under strict control. For example, the primary flight feathers of many rollers (*Coracias*) change in structural colour from deep blue to turquoise in the middle of the vane. In the transition zone between colours, one can see that individual medullary cells faithfully produce either the deep blue or turquoise colour. The structural colour transition across the wing is accomplished with a mosaic of cells with two distinct colours rather than a series of cells that gradually transition between the two colours.

Thus, it appears that the medullary cells physiologically control the conditions necessary to initiate self-assembly, but that the deterministic physical process of self-assembly leaves little opportunity for subsequent variation in the outcome of development. Although additional features of these feathers—such as the shape, thickness and surface of the barb cortex, the distribution of melanosomes and the presence and concentration of carotenoid pigments—may influence the colour produced by the feather, the self-assembly of the nanostructure itself reduces the potential for condition-dependent trait expression in structural coloration during feather development.

We thank Drs Tom Pollard and Andrew Miranker for their helpful comments, and the organizing committee of the 2008 Iridescence Conference at Arizona State University for the invitation to participate. Financial support for this research was provided by Yale University, and grants from the National Science Foundation to R.O.P. (DBI-0078376) and E.R.D. (CAREER CBET-0547294). VIREO gave permission to reproduce the photo in figure 2*a* by T. Laman.

REFERENCES

Aarts, D. G. A. L. & Lekkerkerker, H. N. W. 2004 Confocal scanning laser microscopy on fluid–fluid demixing colloid–polymer mixtures. *J. Phys. Condens. Matter* **16**, S4231–S4242. (doi:10.1088/0953-8984/16/38/035)

Alibardi, L. 2002 Keratinization and lipogenesis in epidermal derivatives of the zebra finch, *Taeniopygia guttata castanotis* (Aves, Ploecidae) during embryonic development. *J. Morphol.* **251**, 294–308. (doi:10.1002/jmor.1090)

Alibardi, L. 2005 Cell structure of developing barbs and barbules in downfeathers of the chick: central role of barb ridge morphogenesis for the evolution of feathers. *J. Submicrosc. Cytol. Pathol.* **37**, 19–41.

Amundson, R. 2001 Adaptation, development, and the quest for common ground. In *Adaptationism and optimality*

(eds S. Hecht Orzack & E. Sober), pp. 303–334. New York, NY: Cambridge University Press.
Amundson, R. 2005 *The changing role of the embryo in evolutionary thought: roots of evo-devo*. Cambridge, UK: Cambridge University Press.
Andersson, M. 1994 *Sexual selection*. Princeton, NJ: Princeton University Press.
Auber, L. 1971/1972 Formation of 'polyhedral' cell cavities in cloudy media of bird feathers. *Proc. R. Soc. Edinb.* **74**, 27–41.
Brush, A. H. 1978 Feather keratins. In *Chemical zoology*, vol. 10 (ed. A. H. Brush), pp. 117–139. New York, NY: Academic Press.
Brush, A. H. 1983 Self-assembly of avian φ-keratins. *J. Protein Chem.* **2**, 63–75. (doi:10.1007/BF01025168)
Brush, A. H. 1993 The origin of feathers. In *Avian biology*, vol. 9 (ed. D. S. Farner, J. S. King & K. C. Parkes), pp. 121–162. London, UK: Academic Press.
Deegan, R. D., Bakajian, O., Dupont, T. F., Huber, G., Nagel, S. R. & Witten, T. A. 1997 Capillary flow as the cause of ring stains from dried liquid drops. *Nature* **389**, 827–829. (doi:10.1038/39827)
Durrer, H. & Villiger, W. 1967 Bildung der Schillerstruktur beim Glanzstar. *Zeitschrift für Zellforschung* **81**, 445–456. (doi:10.1007/BF00342767)
Dyck, J. 1976 Structural colours. *Proc. Int. Ornithol. Congr.* **16**, 426–437.
Dyck, J. 1978 Olive green feathers: reflection of light from the rami and their structure. *Anser* **3**(Suppl.), 57–75.
Erlebacher, J., Aziz, M. J., Karma, A., Dimitrov, N. & Sieradzki, K. 2001 Evolution of nanoporosity in dealloying. *Nature* **410**, 450–453. (doi:10.1038/35068529)
Ghiradella, H. 1974 Development of ultraviolet-reflecting butterfly scales: how to make an interference filter. *J. Morphol.* **142**, 395–410. (doi:10.1002/jmor.1051420404)
Ghiradella, H. 1989 Structure and development of iridescent butterfly scales: lattices and laminae. *J. Morphol.* **202**, 69–88. (doi:10.1002/jmor.1052020106)
Gould, S. J. & Lewontin, R. C. 1979 The spandrels of San Marco and the Panglossian paradigm: a critique of the adaptationist programme. *Proc. R. Soc. B* **205**, 581–598. (doi:10.1098/rspb.1979.0086)
Hemsley, A. R. & Griffiths, P. C. 2000 Architecture in the microcosm: biocolloids, self-assembly and pattern formation. *Phil. Trans. R. Soc. A* **358**, 547–564. (doi:10.1098/rsta.2000.0545)
Hemsley, A. R., Collinson, M. E., Kovach, W. L., Vincent, B. & Williams, T. 1994 Role of self-assembly in biological systems: evidence from iridescent colloidal sporopollenin in *Selaginella* megaspore walls. *Phil. Trans. R. Soc. B* **345**, 163–173. (doi:10.1098/rstb.1994.0095)
Hemsley, A. R., Jenkins, P. D., Collinson, M. E. & Vincent, B. 1996 Experimental modeling of exine self-assembly. *Bot. J. Linn. Soc.* **121**, 177–187. (doi:10.1006/bojl.1996.0031)
Hemsley, A. R., Vincent, B., Collinson, M. E. & Griffiths, P. 1998 Simulated self-assembly of spore exines. *Ann. Bot.* **82**, 105–109. (doi:10.1006/anbo.1998.0653)
Jones, R. A. L. 2002 *Soft condensed matter*. Oxford, UK: Oxford University Press.
Lucas, A. M. & Stettenheim, P. R. 1972 *Avian anatomy—integument*. Washington, DC: US Department of Agriculture Handbook.
Matulionis, D. H. 1970 Morphology of the developing down feathers of chick embryos. *Zeitschrift für Anatomie und Entwicklungsgeschichte* **132**, 107–157. (doi:10.1007/BF00523275)
Neville, A. C. 1975 *Biology of the arthropod cuticle*. New York, NY: Springer.
Neville, A. C. 1993 *Biology of fibrous composites*. Cambridge, UK: Cambridge University Press.
Niklas, K. J. 1992 *Plant biomechanics: an engineering approach to plant form and function*. Chicago, IL: Chicago University Press.
Parker, A. R. 1999 Invertebrate structural colours. In *Functional morphology of the invertebrate skeleton* (ed. E. Savazzi), pp. 65–90. London, UK: Wiley.
Prum, R. O. 1999 Development and evolutionary origin of feathers. *J. Exp. Zool.* (*Mol. Dev. Evol.*) **285**, 291–306. (doi:10.1002/(SICI)1097-010X(19991215)285:4<291::AID-JEZ1>3.0.CO;2-9)
Prum, R. O. 2006 Anatomy, physics, and evolution of avian structural colors. In *Bird coloration*, vol. 1 (eds G. E. Hill & K. J. McGraw). Mechanisms and Measurements, pp. 295–353. Cambridge, MA: Harvard University Press.
Prum, R. O. & Torres, R. H. 2003 A Fourier tool for the analysis of coherent light scattering by bio-optical nanostructures. *Integr. Comp. Biol.* **43**, 591–602. (doi:10.1093/icb/43.4.591)
Prum, R. O. & Williamson, S. 2001 A theory of the growth and evolution of feather shape. *J. Exp. Zool.* (*Mol. Dev. Evol.*) **291**, 30–57. (doi:10.1002/jez.4)
Prum, R. O., Torres, R. H., Williamson, S. & Dyck, J. 1998 Coherent light scattering by blue feather barbs. *Nature* **396**, 28–29. (doi:10.1038/23838)
Prum, R. O., Torres, R. H., Williamson, S. & Dyck, J. 1999 Two-dimensional Fourier analysis of the spongy medullary keratin of structurally coloured feather barbs. *Proc. R. Soc. B* **266**, 13–22. (doi:10.1098/rspb.1999.0598)
Prum, R. O., Cole, J. & Torres, R. H. 2004 Blue integumentary structural colours of dragonflies (Odonata) are not produced by incoherent Tyndall scattering. *J. Exp. Biol.* **207**, 3999–4009. (doi:10.1242/jeb.01240)
Srinivasarao, M. 1999 Nano-optics in the biological world: beetles, butterflies, birds, and moths. *Chem. Rev.* **99**, 1935–1961. (doi:10.1021/cr970080y)
Takenaka, M. & Hashimoto, T. 1992 Scattering studies of self-assembling processes of polymer blends in spinodal decomposition. II. Temperature dependence. *J. Chem. Phys.* **96**, 6177–6190. (doi:10.1063/1.462635)
Thompson, D. A. W. 1917 *On growth and form*. Cambridge, UK: Cambridge University Press.
Tsapis, N., Dufresne, E. R., Sinha, S. S., Riera, C. S., Hutchinson, J. W., Mahadevan, L. & Weitz, D. A. 2005 Onset of buckling in drying droplets of colloidal suspensions. *Phys. Rev. Lett.* **94**, 018 302. (doi:10.1103/PhysRevLett.94.018302)
Vogel, S. 2003 *Comparative biomechanics: life's physical world*. Princeton, NJ: Princeton University Press.
Vukusic, P. & Sambles, J. R. 2003 Photonic structures in biology. *Nature* **424**, 852–855. (doi:10.1038/nature01941)
Wake, D. B. 1991 Homoplasy: the result of natural selection, or evidence of design limitations? *Am. Nat.* **138**, 543–567. (doi:10.1086/285234)